An Adaptive Entropic Thresholding Technique for Image Processing and Diagnostic Analysis of Microcirculation Videos

Nazanin Mirshahi,
Kayvan Najarian
Dept. of Computer
Science
VCU
Richmond, VA, USA
mirshahin@vcu.edu,
knajarian@vcu.edu

Sumeyra Demir,
Rosalyn Hobson
Dept. of Electrical
Engineering
VCU
Richmond, VA, USA
demirsu@vcu.edu,
rhobson@vcu.edu

Kevin Ward
Dept. of Emergency
Medicine

VCURES
Richmond, VA, USA
krward@vcu.edu

Roya Hakimzadeh

Signal Processing
Technologies LLC

Richmond, VA, USA
contact@signalproces
singtechnologies.com

Abstract – **Understanding the functionality of microcirculation is a key factor in the analysis of blood circulatory system. The blood flow distribution changes, based on the physiological effects of disorders. This study presents a method for analysis of microcirculation videos captured from lingual surface of 10 animal subjects. The technique applies advanced image processing methods to stabilize videos, segment microvessels (capillaries and small blood vessels), and estimate the average Functional Capillary Density on 20 consecutive frames for each subject. The algorithm consists of four main parts: pre-processing, video stabilization, entropic-based adaptive local thresholding segmentation and post-processing. The key objective is to quantitatively examine the changes that occur in microcirculation over treatment periods for diseases as well as for the resuscitation process. The designed system will help physicians and medical researchers in diagnostic and therapeutic decision making to determine the sufficiency of resuscitation process and the effect of drug consumption in patients. In particular, the system focuses on minimizing user interaction while improving the accuracy of the analysis. Visual evaluation of the results by medical experts indicates that the technique is capable of identifying 95% of active capillaries and blood vessels in videos.**

Keywords - Microcirculatin, Image processing, multi-resolution, entropic thresholding, Adaptive local thresholding, Lorentz information measure

I. INTRODUCTION

Microcirculation refers to the blood flow in blood vessels less than 100 μm luminal diameter [2]. Changes in microcirculation might be due to numerous diseases and abnormalities in humans. Microcirculatory studies indicate that the small diameter of microvessels (arterioles, capillaries and venules) helps observe changes in blood circulation more evidently compared to large blood vessels. Basically, the rheological properties of blood in capillaries and small blood vessels lead to effective viscosity in those vessels which considerably differentiates the circulation of red blood cells and plasma in microvessels and large blood vessels. The major function of the micro-vascular network is distribution of nutrients, fluid and oxygen throughout tissues in humans [3,4]. As a result, the distributions of microcirculatory network and blood circulation are considered to be key factors in human physiological health [5-8]. Evidence suggests that information regarding the status of microcirculation plays a crucial role in treatment and diagnosis of several diseases such as sepsis, sickle cell, chronic ulcers, diabetes mellitus and hypertension [9-13]. Research and clinical experience show that each of the mentioned diseases uniquely affects characteristics of microcirculation such as structure of capillaries and features of blood flow [14-18]. Hence, investigation of microcirculatory changes has clinical significance in measurement and observation of the changes in response to treatment of microvessels under clinical conditions. Timely detection of such changes potentially helps in taking proper actions which in turns improves the chances of treatment success. A technique to quantitatively assess and monitor these alterations is extremely valuable for further study of such pathological conditions [19]. Particularly, in trauma care, continuous monitoring of microcirculation and measurement of microcirculation indices while resuscitation process helps in determining when to start/stop resuscitation [20-22].

The recent development of videomicroscopy technology has provided effective tools for detection and assessment of tissue perfusion and oxygenation through visualization of microvasculature [23]. Quantitative analysis of microcirculation allows monitoring changes in microvessels that occur due to diseases and other abnormalities. Both visual analysis and use of existing semi-automated video analysis tools are time-consuming and demanding, preventing real-time assessment of microcirculation. This calls for

automated systems to be used for applications including resuscitation.

Two prevalent medical imaging techniques that have been widely used for examining microcirculation during surgery and for other clinical research are Orthogonal Polarization Spectral (OPS) imaging and Side-stream Dark Field (SDF) [24,25]. SDF is superior to OPS in the field of microcirculation study as it improves contrast and lowers surface reflectance compared to OPS [35]. Although advances in hardware systems have played a major role in acquiring knowledge about the physiology and pathology of microvascular function, lack of existing techniques for rapid and accurate processing of microcirculation videos is still an issue. Manual analysis of this information by experts is a complex and time-demanding process which may not be used for real-time assessment of microcirculation; however, an automated system can therapeutically and diagnostically assist physicians and medical researchers.

Several methods have been employed to analyze microcirculation images. A short version of the method proposed in this paper was mentioned in [1]. Dobbe et al. has proposed a semi-automatic, highly accurate method for the analysis of microcirculation [26]. The method applies image stabilization, centerline detection and space time diagram to detect capillaries and small blood vessels. Despite the high accuracy, this method is extremely time-consuming and requires human interaction to produce acceptable results, and therefore, it is not appropriate for real-time applications of microcirculation analysis. The image processing techniques that were proposed in the field of microcirculation are mainly used to process high quality color and/or grayscale retinal images; conversely, the accuracy of the results declines when the same method is applied to other microcirculation images due to their low contrast. Numerous techniques and their combinations have been employed on segmentation of small blood vessels. Pattern recognition-based techniques were used by Staal et al. to analyze two-dimensional color images of retina [27]. Several features of the image are selected and classified to extract image ridges automatically. The main shortcoming of this method is that it is likely to over- and undersegment the vessels. The tracking-based approach described in [28] locates the optic nerve in ocular fundus images. Utilizing fuzzy convergence of the blood vessel, the algorithm uses two features, convergence of vessel network and brightness of the nerve to perform segmentation. Despite its capabilities, the method fails to accurately detect blood vessels where bright lesion regions exist. Vermeer et al. applied a model based approach [29].

The method incorporates Laplace concept, thresholding as well as classification to detect vessels in retinal images. The method requires high levels of human intervention, therefore, is not appropriate for real-time segmentation of microcirculation images. Artificial intelligence methods use prior knowledge for direct segmentation [30].

Most of the vessel segmentation methods that were reviewed earlier in this section are capable of extracting vessels in retinal images; however, lack essential properties to segment microcirculation images [31]. The aim of the proposed study is to stabilize and segment low local contrast microcirculation videos automatically, accurately and in a close to real-time manner in order to aid physicians and clinical researchers in making diagnostic and therapeutic decisions. This algorithm attempts to eliminate human intervention in the precise extraction of small blood vessels. Furthermore, it calculates the diagnostically useful measure of Functional Capillary Density (FCD) for 20 consecutive frames in a microcirculation video [34]. The algorithm segments the image using a modified entropic thresholding technique [33]. Entropy-based methods apply a threshold to the images using entropy of an image or similar information. The rest of thresholding techniques are categorized into five main classes [36]. In histogram shape-based methods, certain parts of image histogram are assessed. Clustering-based methods utilize mixture of two Gaussians to separate foreground and background in an image. Object attribute-based algorithms look at similarities between the original image and its corresponding binary image. Higher order probability distribution is used in thresholding based on spatial methods. Local methods use local image properties to threshold an image. Experiments have shown that for the purpose of thresholding microcirculation images, entropic thresholding techniques yield the most successful outputs.

Section II provides a detailed description of the methodology including preprocessing, video stabilization, segmentation and post-processing. The results of the study on 10 video samples of hemorrhaged and healthy subjects are presented in Section III. Section IV contains the conclusion and discussion of the obtained results. Finally, Section V concludes the paper with future work.

II. METHODOLOGY

The proposed methodology is an extension of [1]. Key modifications were applied to improve the segmentation part. Furthermore, the algorithm was examined on more data samples to evaluate the capabilities of the technique in this paper. The

microcirculation videos used to validate the results of the proposed research study are based on SDF imaging technique, captured by MicroScan hardware [35]. MicroScan is an easy to use instrument that is mainly utilized in various microcirculation observations and analysis.   The data samples for this study were acquired from sublingual surface of healthy and hemorrhaged swine subjects. In SDF imaging modality, the light from light emitting diodes is absorbed by hemoglobin, which results in the visibility of flowing cells. Consequently, the walls of the capillaries become visible in the presence of Red Blood Cells (RBCs) [24]. Medical research has proven that lingual surface suffice for the investigation of microcirculation condition in the body as capillaries are adequately superficial for MicroScan. Thus, lingual recordings are considered valid indicators of normality or abnormalities of the microcirculatory network.

A major challenge in the image processing of microcirculation videos are their low resolution and local contrast that complicates the distinction between objects of interest (capillaries and small blood vessels) and frame background. An instance of an original microcirculation frame is provided in Figure 2. Another challenge is the inconsistency of the graylevel intensity in background and blood vessels from one sample to another. The effect of uneven lighting due to the movement of camera and/or subjects results in different levels of intensity in different frames. Therefore, the choice of a single threshold level for an entire frame is not adequate for effective thresholding. The proposed study addresses the mentioned issues by adopting an adaptive entropic thresholding technique.

Prior to being processed, videos are converted to their comprising sets of images or frames; these frames were either processed individually or in combination with other frames as will be described in the rest of the paper. An outline of different steps of the algorithm is provided in Figure 1.
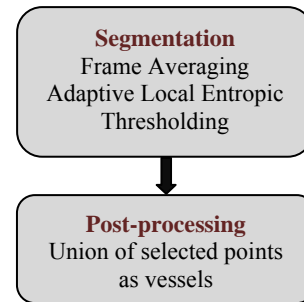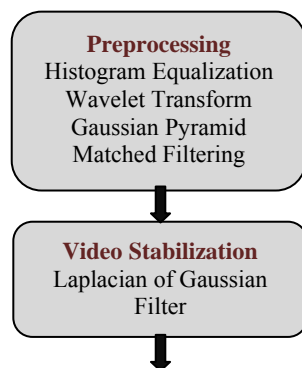

Figure1. Block diagram of the algorithm

A. PREPROCESSING

Preprocessing of microcirculatory images is essential considering the low local contrast of microcirculation images. Preprocessing usually comprise a series of operations to improve the quality of images in order to maximize the difference between image background and objects of interests. In microcirculation images, the intensity of capillaries and small blood vessels are exceptionally close to that of background and tissues. In order to process the images, the first main step is preprocessing.

As the first step, adaptive histogram equalization is applied to the images to help enhance low local contrast of the images. The histogram of an image is a representation for the number of different pixel values in the image. Microcirculation images comprise of a narrow range of intensities. In adaptive histogram equalization, the histogram for various parts of the image is generated and interpolated. Bilinear interpolation eliminates the visibility of the boundary lines that were produced by local histograms. The result of adaptive histogram equalization is a modified image whose histogram is different from that of the original image. In other words, the background appears rather uniform in terms of intensity with a remarkable contrast as compared to the blood vessels and other artifacts in the image.

To further reduce the effects of background noise, wavelet transformation is incorporated in this step. Wavelet transformation decomposes the image into its different frequency contents. Usually, high frequencies represent noise and low frequencies represent details in an image. The image is transformed to wavelet domain and decomposed with mother wavelet of Daubechies 8, level 2.   Following that, high frequencies present within the image are filtered.   Then the image is reconstructed in the original domain. The noise in the resulting image is much lesser than the input image.

A microcirculation frame usually contains blood vessel in different levels of proximity to the surface of tongue. Representing images in multiple spatial-

frequency domains emphasizes the patterns of blood vessels in different scales that normally can not be seen in the image. The significance of analyzing images at various resolutions is that the objects of different sizes are more visible in different resolution levels. Experiment shows that level 2 and level 3 of Gaussian pyramid separate blood vessels of different sizes, thus making the segmentation a more accurate process. To construct the first level of Gaussian Pyramid, image is filtered using a low-pass filter and then sub-sampled. Low-pass filter presents an equivalent effect as convolving images with a series of Gaussian-like weighting functions followed by sub-sampling. The same procedure is repeated, using the resulting image of the earlier step as an input image to generate the next set of results. The filter operates as convolution of Gaussian blur kernel with the image to eliminate high frequencies components. The pyramid compresses image by making it coarser in each level and reducing the number of bits of precision. The blood vessels become more distinguishable after this step. In this study, for each frame, levels 2 and 3 of Gaussian Pyramid are saved for future analysis.

Matched filter is applied to the image to extract features. In this step, to enhance the edges of blood vessels, matched filter is applied to the image [32]. Matched filter approximates the intensity profile of the image with Gaussian curves. In this study, the function in equation (1) is implemented for the detection of linear anti-parallel pieces of blood vessels. Although the gray-level profile varies for different vessels, similar properties of blood vessels make the mentioned Gaussian function appropriate for this purpose. The function is a two-dimensional kernel that is convolved with the image to sharpen edges of blood vessels.

$$f(x, y) = e^{(\frac{-x^2}{2\delta^2})} \text{ for } |y| \leq \frac{L}{2} \tag{1}$$

In (1), L represents the size of the selected slice of the vessel with fixed orientation. The value of L is specified by experiment. The kernel is originally only aligned with y-axis. In order for the kernel to detect vessels in other orientations, the kernel is rotated. The rotation is performed convolving ten 15×16 pixel kernels with the image. The maximum value resulting from each convolution is considered the convolution response of that orientation. This step of the algorithm enhances the edges of blood vessels, while blurring large blood vessels and tissue. An instance of this effect is illustrated in Figure 3.

B. VIDEO STABILIZATION

Recording videos from microcirculation provides an effective tool to visualize the activity of blood vessels and capillaries over a short period of time. This makes video superior to image when analyzing microcirculatory networks, since video contains more information compared to image. Despite the advantages of capturing videos for the study of microcirculation, the motion artifact due to the movement of the handheld camera and that of the subject are obstacles for effective analysis of microcirculation videos. To eliminate the effects of motion artifacts, video stabilization is performed at this step.

The main aim of this step is to calculate the transformation between two consecutive frames in the video. The first step is to compute the first derivatives of the image using Gaussian Gradient filter. Since the image is a function of two variables, $f(x, y)$, the derivatives are computed in both horizontal and vertical direction. The sum of the resulting values of the filter in each direction generates the overall Gaussian gradient for the image. Following that, seven control points are selected in the first frame. The control point should be on the vessels and not on the background in order to be tracked effectively. Laplacian of Gaussian filter is applied to the frame for choosing the most relevant control points. Laplacian of Gaussian filter computes the second order derivatives of the Gaussian function. The filter is used to find regions of rapid change in images such as edges. Using the filter guarantees that the selected points are located on the objects of interest. The control points are the ones that yield to the highest amounts of filter output. Once being picked for the first frame, control points are tracked in the 19 following frames. To track the same points in the following frames, a window of *25x25* pixels is defined around the control point. The points are tracked within a corresponding window of *65x65* size in the following frames. In case any of the point is fallen outside the image due to excessive motion, new control points will be defined using the mentioned method.

The next step is to calculate the cross-correlation coefficients between two successive frames. Cross-correlation coefficients are calculated for tracking the points in the previous step. To identify the control points in the frames except for the first frame, the *65x65* window is scanned to detect the maximum correlated regions in two consecutive frames. The frames are registered according to the maximum correlated sub-areas. Registration helps finding the amount of shift between the two successive frames. In

other words, the distance between the frames is acquired through calculating the cross-correlation value. $d(f_i, f_{i+1})$ represents the distance between the grayscale profile of two succeeding image in which i shows the frame number. This value will be used as a parameter in segmentation. An example of the stabilization result for 10 frames is shown in Figure 4.

C. SEGMENTATION

Image segmentation is performed to partition image into its comprising components. The objective of microcirculation image processing is to separate background from blood vessels and capillaries using grayscale values. Such separations make the analysis of the image an easier task. The outcome of segmentation is a binary image whose background is shown with white pixels and objects of interest with black pixels.

One main class of techniques that is incorporated for image segmentation is thresholding. The main classes of thresholding were mentioned in the introduction part. Depending on the application, one may use global thresholding or local thresholding. Uneven grayscale intensity of the background and the varieties in the intensity of the objects in microcirculation images make the global thresholding inefficient. However, local thresholding smoothly varies across the image and is capable to adapt the threshold value for different parts of the image. This study adaptively selects windows in the image based on Lorentz Information Measure (LIM) [37]. Following that, for the thresholding of each sub-image, the algorithm implements an extension of the entropic thresholding technique proposed in [33].

Adaptive local thresholding successfully reduces the issue with uneven background intensity by partitioning the image into windows of variable sizes based on LIM value. If the image F is the gray level image and $f(x, y)$ is defined as the intensity image, the amount of information in the image known as Picture Information Measure (PIM) is calculated by:

$$PIM(f) = \sum_{i=0}^{F-1} h(i) - \max h(i) \qquad (2)$$

PIM shows the minimal graylevel variation if $f(x, y)$ is converted to a constant grayscale image. $h(i)$ shows the graylevel histogram of the image for $h : \{0, 1, ..., F-1\} \to N$. If the image comprises of only one graylevel, $PIM(f) = 0$, while $PIM(f) = \max$

occurs when the graylevel intensity of the image is uniformly distributed.

The normalized form of (1) is defined as:

$$NPIM(f) = PIM(f) / N(f) \qquad (3)$$

where $N(f)$ is the number of pixels in the image. $NPIM(f)$ can be calculated for any sub-image in the image, indicating the amount of information in the given sub-image. An experimental cutoff value for $NPIM(f)$ is chosen in order to adaptively adjust the sub-image size for thresholding. The values greater than the cutoff value ensure that the sub-images contain both background and objects of interest.

The superiority of thresholding method in the proposed algorithm is that it considers flow information in addition to local property and intensity information. The technique is based on graylevel spatial correlation histogram of the image. The aim is to maintain the spatial structure of the image using pixel neighborhood property. In an image F with graylevel intensity of $f(x, y)$ in which (x, y) represents the coordination of a pixel, let $Q \times R$ be the number of pixels. $g(x, y)$ is defined as the number of pixels in $N \times N$ neighborhood of pixel (x, y) within ζ distance of the pixel. The ζ value of 2 and neighborhood of 3×3 ($N = 3$) were chosen empirically for the purpose of this study.

The flow factor used in this part was calculated in the stabilization section. For every frame, the summation of the differences between each consecutive pair frames in 10 preceding frames is computed using the following equation:

$$Sd(f) = \sum_{n=i-10}^{n=i} d(f_n, f_{n+1}) \qquad (4)$$

Three parameters of flow, neighborhood vicinity and pixel intensity information are used in equation (5) to calculate the graylevel spatial correlation histogram of the image:

$$h(k, m, D) = prob(f(x, y) = k, g(x, y) = m, \\ Sd(f) = D) \qquad (5)$$

Equation (5) determines the probability $h(k, m, D)$ in which $f(x, y) = k$, $g(x, y) = m$ and $Sd(f) = D$ where $0 \le k \le 255$, $1 \le m \le 9$ and $1 \le D \le 2$.

According to the principle of entropy, noise and edge produce more information than background and

objects. In order to emphasize the effect of *m* as a key distinction factor, the nonlinear function in equation (6) is multiplied with entropy function.

$$W(m,N) = (1 + e^{\frac{-9m}{N \times N}}) / (1 - e^{\frac{-9m}{N \times N}}) \qquad (6)$$

In equation (6), N is the selected neighborhood of a pixel and *m* is the number of neighbor pixels within ζ distance of the pixel, $m = \{1, 2, 3, ..., NxN\}$.

In the next step, threshold *T* is calculated; *T* is $0 < T < l - 1$. It segments the image into object and background, represented by *O* and *B* respectively. In order to calculate *T*, the second order entropy of image and background is calculated using equations (7) and (8).

$$(7)$$
$$H_B^{(2)}(T,N) = -\sum_{k=T+1}^{255} \sum_{m=1}^{N \times N} \frac{P(k,m,D)}{P_B(T)} \ln(\frac{P(k,m,D)}{P_B(T)}) W(m,N)$$

$$(8)$$
$$H_O^{(2)}(T,N) = -\sum_{k=0}^{T} \sum_{m=1}^{N \times N} \frac{P(k,m,D)}{P_O(T)} \ln(\frac{P(k,m,D)}{P_O(T)}) W(m,N)$$

In the equations of second order entropy, $P(k,m,D)$ is the normalized form of $h(k,m,D)$.

The optimal threshold is calculated as the total of equations (7) and (8). The optimal threshold is calculated using:

$$H(T,N) = H_O^{(2)}(T,N) + H_B^{(2)}(T,N) \qquad (9)$$

T is obtained by computing a value that maximizes *H(T,N)*. Experimental evidence has shown that as a result of noise factors, the obtained value is not the optimal threshold. In order to eliminate this issue, the median of ten maximum values of *H(T,N)* is selected to be the optimal threshold.

The final segmentation process employs the information acquired through calculation of Lorentz Information Measure to threshold the image using the mentioned entropic thresholding technique. As mentioned in the stabilization part, 20 frames are stabilized for each level of the Gaussian Pyramid. The output of the stabilization is a set of stabilized frames that demonstrate active blood vessels. In many instances, stabilization distorts the edges of the frames

to effectively smooth out the video. In order to eliminate the possible effect of the stabilization, 15 pixels from top, bottom, right and left of the images are removed. Following that, the intensity values of each pixel coordinate in 20 stabilized frames are arithmetically averaged. The result of this step is the input for the main segmentation part.

The size of microcirculation images of the study after removing a 15 pixel frame from the image becomes *450x690* pixels. The original window size of *60x60* pixels is chosen empirically to divide the image into sub-images for thresholding. Thresholding starts with the original window size from the top left of the image. The image is partitioned into a window of size *60x60* pixels and $NPIM(f)$ is calculated for the sub-image. If the $NPIM(f)$ value was greater than 0.97, the sub-image is thresholded using the mentioned entropic thresholding technique. The limit value for $NPIM(f)$ was selected experimentally. If the $NPIM(f)$ value is less than the limit, the window size adaptively grows to *120x120*, twice as much as the original window in direction of *x* and *y*. The sub-image is then thresholded using the proposed entropic thresholding technique. The same process of thresholding the sub-images is repeated for the entire image. The output of thresholding is a binary image in which blood vessels and capillaries are represented by black pixels and the background with white pixels.

Despite the success of pre-processing to reduce the effect of image artifacts, the result of this step might still contain tissue and other artifacts in shape of scattered small objects. One solution to eliminate the effect of artifacts is to apply morphological operations to the image. Morphology performs mathematical techniques on images to analyze and process geometrical shapes. In this step, the objects in the binary image are labeled. The size, width and length of the objects are acquired and compared to the user defined ones. The objects with values out of the defined range are removed. Such operation clears the image from isolated pixels with width and length less than 4 and 10 pixels as well as large vessels with width of greater than 30 pixels. The result of this step is a binary image with less noise.

D. POST-PROCESSING

Post-processing refers to a combination of techniques for generating the final results of the algorithm. In the previous steps, levels 2 and 3 of Gaussian pyramid were generated for 20 frames. Following that, the frames were stabilized, averaged

and segmented for each level. Accordingly, two sets of images were acquired.

Different levels of Gaussian pyramid provide different resolution of the same image. Since different blood vessels might be better visible in each of the levels, there is a need to combine the results of the two levels to construct the final results. The union of points identified as capillaries and blood vessels in each set forms the ultimate results of the algorithm. The final result is an image that shows the active blood vessels.

III. RESULTS

To verify the effectives of the proposed algorithm, it was tested on 10 microcirculation video samples. Five of the subjects were hemorrhaged animals and five were healthy animal subjects. Equal number of normal and abnormal subjects helps examining the major difference in statistical analysis of the results. The videos were captured with the rate of 30 frames per second. The original size of a video frame is 480x720 pixels. The sample data were provided by Virginia Commonwealth University Reanimation Engineering Shock Center.

The algorithm was applied to the first 20 frames of each video. The results of different steps of the algorithm for a healthy case are illustrated in Figures 2-5, while Figures 6-9 show the results for a hemorrhaged case. MATLAB® programming language was used to develop codes to examine the validity of the proposed algorithm and to generate experimental results. With respect to time complexity, the algorithm takes an average of 15 minutes to run on a 2.40 GHz computer with 3 GB of RAM. The evaluation of results is performed through visual inspection of medical experts. The inspection has shown that the accuracy of algorithm in extracting active blood vessels and capillaries is 95% on average.

The measure of FCD was calculated for the sample data. The FCD value results are listed in Table 1. FCD is the area of the segmented capillaries in an image divided by the area of the image [33]. In each averaged frame, the total number of black pixels is divided by the size of the image to obtain FCD value. The result shows that the algorithm can successfully distinguish between normal and abnormal cases based on a simple statistical analysis.

IV. CONCLUSION

The proposed method is a fully automated approach for image processing of microcirculation videos. The algorithm incorporates a novel thresholding technique that considers flow information to be a key factor in calculation of entropy. Furthermore, it adjusts the threshold level locally based on image information using Lorentz Information Measure. The algorithm looks at two levels of Gaussian Pyramid resolutions to acquire a true estimate of active blood vessels in a video. The technique is capable of distinguishing between the healthy and hemorrhaged subjects in the 10 studied samples using Functional Capillary Density. Visual evaluation of the results shows 95% accuracy in blood vessel detection. The designed technique can potentially assist physicians and medical researchers in making diagnostic decisions.

V. FUTURE WORK

As future work, an extension of the current approach will combine multi-resolution concept with multi-thresholding to improve the segmentation results while reducing the false positives. Other diagnostically useful measures such as Perfused Vessel Density (PVD), Proportion of Perfused vessels (PPV) and Microvascular Flow Index (MFI) will be calculated using the proposed algorithm. A larger dataset will be acquired and the algorithm will be tested and validated on the new dataset. The stabilization technique will be improved and combined with other registration techniques. The results will be validated using the available semi-automated commercial software tools such as Vascular Analysis Commercial software tools by medical experts. Statistical analysis will be performed for further evaluation of the results.

Table1. FCD for five healthy and five Hemorrhaged subjects

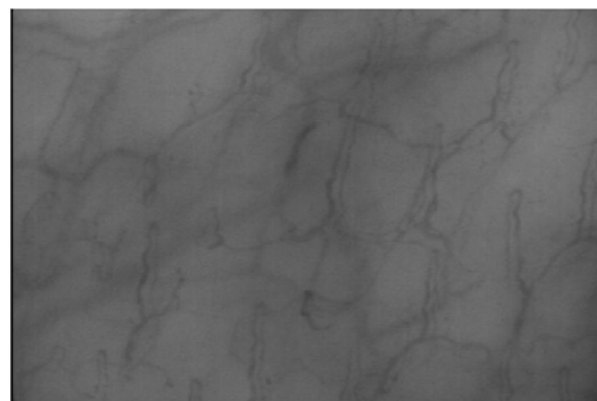|	Healthy	Hemorrhaged
Case 1	0.12	0.09
Case 2	0.15	0.08
Case 3	0.14	0.05
Case 4	0.10	0.05
Case 5	0.12	0.07

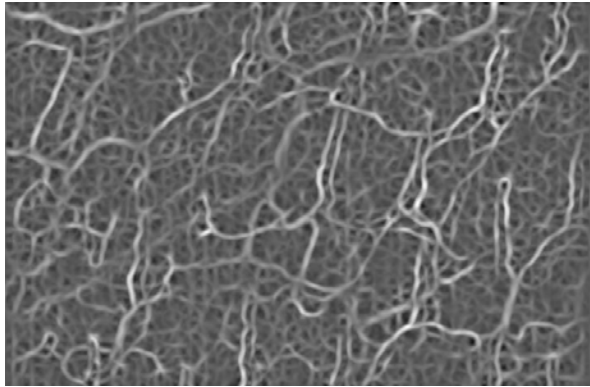Figure 2. Original image of a frame– Healthy subject

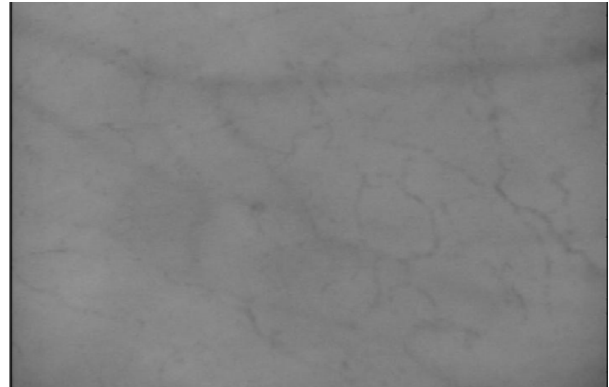Figure 3. Preprocessing of the frame in Fig2, level 3 of Gaussian Pyramid – Healthy subject

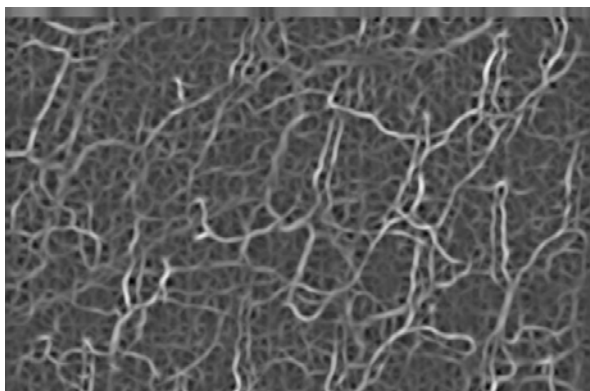Figure 6. Original image of a frame – Hemorrhaged subject

Figure 4. Stabilization results of 10 consecutive frames (Fig2 as the first frame), level 3 of Gaussian Pyramid - Healthy subject
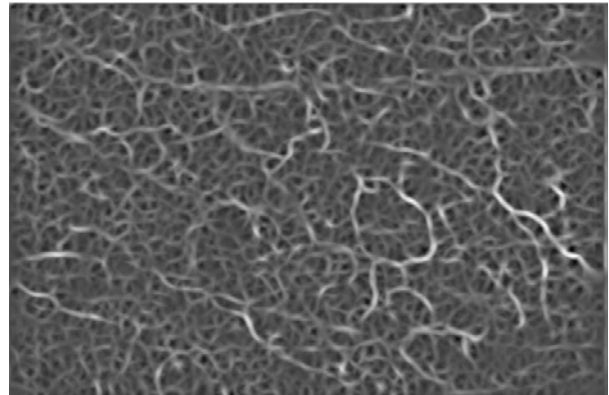

Figure 7. Preprocessing of the frame in Fig6, level 3 of Gaussian Pyramid – Hemorrhaged subject

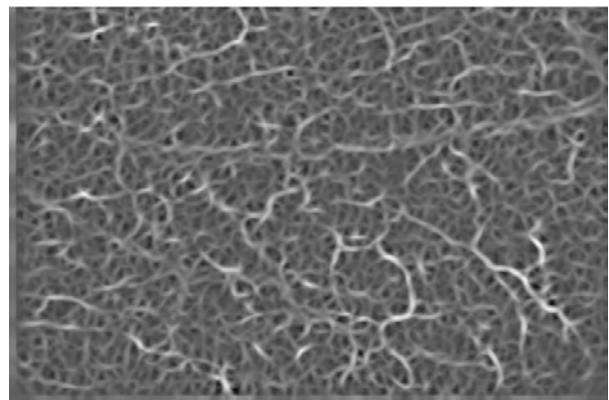Figure 5.Postprocessing results of 20 frames – Healthy subject

Figure 8. Stabilization results of 10 consecutive frames (Fig7 as the first frame), level 3 of Gaussian Pyramid - Hemorrhaged subject

Figure 9.Postprocessing results of 20 frames - Hemorrhaged subject

ACKNOWLEDGEMENT

REFERENCES

[1] N. Mirshahi, S.Demir, K. Ward, R. Hobson, R. Hakimzadeh, K. Najarian, "A Multi-resolution Entropic-Based Image Processing Technique for Diagnostic Analysis of Microcirculation Videos," *biosciencesworld, pp.64-69,* The First International Conference on Biosciences, 2010

[2] R. F. Tuma, W. N. Duran, K. Ley. *HANDBOOK OF PHYSIOLOGY MICROCIRCULATIO,* Elsevier Science, USA, 2008.

[3] AR. Pries, D. Neuhaus and P. Gaehtgens, "Blood viscosity in tube flow: dependence on diameter and hematocrit." *Am J Physiol,* 263: H1770-H1778, 1992.

[4]A. Krogh, *Anatomy and physiology of capillaries*. New Haven Connecticut: Yale University Press, 1929.

[5]A. Krog, "Supply of oxygen to the tissues and the regulation of the capillary circulation." *J physiol (Lond)* 52:457-474, 1919.

[6] AG. Tsai, PC. Johnson and M. Intaglietta, "Oxygen gradients in the microcirculation", *Physiol Rev* 83:993-963, 2003.

[7] CC. Michel and EE. Curry, "Microvascular permeability", *Physiol Rev* 79: 703-761, 1999.

[8] U. Yuan, WM. Chilian, HJ. Granger and DC. Zaeija, "Flow modulates coronary venular permeability by a nitric oxide-related mechanism." *Am J Physiol* 263:H641-H646, 1992.

[9] RM. Bateman, MD. Sharpe, and CG. Ellis, "Bench-to-bedside review: microvascular dysfunction in sepsis: hemodynamics, oxygen transport and nitric oxide" *Crit Care Med 7*: 359–373, 2003.

[10] RP. Hebbel, R. Osarogiagbon, D. Kaul, "The endothelial biology of sickle cell disease; inflammation and chronic vasculopathy" *Microcirculation* 11:129-151, 2004.

[11] MJ. Stuart, and RL. Nagel, "Sickle cell disease", *The Lancent* 364:1343-1360, 2004.

[12] BI. Levy, G. Ambrosio, AR. Pries, and HA. Struijker-Boudier. "Microcirculation in hypertension: a new target for treatment?" *Circulation* 104:735–740, 2001.

[13] C. Verdant, and D. De Backer, "How monitoring of the microcirculation may help us at the bedside", *Curr Opin Crit Care*, 11(3):240-244, 2005.

[14] KA. Nath, ZS. Katusic, and MT. Gladwin, "The perfusion paradox and instability in sickle cell disease", *Microcirculation,* 11:179-193, 2004.

[15] DK. Kaul, and ME. Farby, "In vivo studies of sickle red blood cells", *Microcirculation*: 11:153-156, 2004.

[16] RM. Touyz, "Intracellular Mechanisms Involved in Vascular Remodeling of Resistance Arteries in Hypertension: Role of Angiotensin II", *Exp Physiol*, 90: 499-455, 2005.

[17] EH. Serne, RO. Gans, JC. ter Maaten, GJ. Tangelder, AJ. Donker, and CD. Stehouwer, "Impaired skin capillary recruitment in essential hypertension is caused by both functional and structural capillary rarefaction", *Hypertension*: 38:238-242, 2001.

[18] MA. Creager, TF. Luscher, F. Cosentino, and JA. Bechkman, "Diabetes and Vascular disease: pathophysiology, clinical consequences, and medical therapy: part I", *Circulation* 108:1527-1532, 2003.

[19] O. Genzel-Boroviczeny, J. Strotgen, A. G. Harris, K. Messmer, and F. Christ, "Orthogonal polarization spectral imaging (OPS): A novel method to measure the microcirculation in term and preterm infants transcutaneously", *Pediatr Res* 51:386–391, 2002.

[20] Y. Sakr, MJ. Dubois, D. De Backer, J. Creteur, JL. Vincent, "Persistent microcirculatory alterations are associated with organ failure and death in patients with septic shock", *Crit Care Med*, 32:1825-1831, 2004.

[21] PE. Spronk, C. Ince, MJ. Gardien, KR. Mathura, HM. Oudemans-van Straaten, and DF. Zandstra, "Nitroglycerin in septic shock after intravascular volume resuscitation", *Lancet*, 360:1395-1396, 2002.

[22] M. Fries, M. H. Weil, Y. Chang,, C. Castillo, and W. Tang, "Microcirculation during cardiac arrest and resuscitation", *Crit Care Med* 34: 454–457, 2006.

[23] E. Chaigneau, M. Oheim, E. Audinat, and S. Charpak, *Two Photon imaging of capillary blood flow in olfactory bulb glomeruli.* Proc Natl Acad Sci, USA, 100:13081-13087, 2003.

[24] V. Cerný, Z. Turek, and R. Pařízková, "Orthogonal polarization spectral imaging: a review", *Physiol. Res.* 56, 2007.

[25] C. Ince, "The microcirculation is the motor of sepsis", *Critical Care,* 9(suppl 4):S13-S19, 2005.

[26] J. G. G. Dobbe, G. J. Streekstra, B. Atasever, R. van Zijderveld and C. Ince, "The measurement of functional microcirculatory density and velocity distributions using automated image analysis", *Med Biol Eng Comput*, 46(7): 659–670, 2008.

[27] J. Staal, M. D. Abràmoff, M. Niemeijer, M. A. Viergever, and B. V. Ginneken, "Ridge-Based vessel segmentation in color images of the retina", *IEEE Transactions on Medical Imaging*, vol. 23, no. 4, pp. 501–509, 2004.

[28] A. Hoover, and M. Goldbaum, "Locating the optic nerve in a retinal image using the fuzzy convergence of the blood vessels", *IEEE Tran. on Medical Imaging,* Vol. 22, No. 8, p. 951-958, 2003.

[29] K.A. Vermeer, F.M. Vos, H.G. Lemij, and A.M. Vossepoel, "A model based method for retinal blood vessel detection", Comput. Biol. Med., in press, DOI: 10.1016/S0010-4825(03)00055-6, 2003.

[30] U. Rost, H. Munkel, and C. E. Liedtke, "A knowledge based system for the configuration of image processing algorithms", *Fachtagung Informations und Mikrosystem Technik,* 1998.

[31] C. Kirbas, and F. Quek, "Vessel Extraction Techniques and Algorithms : A Survey" , *Third IEEE Symposium on BioInformatics and BioEngineering*, 2003.

[32] S. Chaudhuri, S. Chatterjee, N. Katz, M. Nelson, and M. Goldbaum, "Detection of blood vessels in retinal images using two dimensional matched filters:' *IEEE Trans. Medical imaging,* vol. 8, no. 3, 1989.

[33] Y. Xiao, Z. Cao, and T. Zhang, "Entropic Thresholding Based on Gray Level Spatial Correlation Histogram", *IEEE Trans. on Wireless Communications 7(1): 334-342,* 2008.

[34] D. De Backer, S. Hollenberg, C. Boerma, P. Goedhart, G. Büchele, G. Ospina-Tascon, I. Dobbe, C. Ince, "How to evaluate the microcirculation: report of a round table condference". *Critical Care*, 11:R101, 2007.

[35] D. Johnson, "Introducing the MicroScan". MicroVision Medical.   July   1,   2010 <http://www.microvisionmedical.com/mvm_docs/MicroScan.pdf>.

[36] S Mehmet, S Bulent, "Survey over image thresholding techniques and quantitative performance evaluation" *Journal of Electronic Imaging*, 2004.

[37] S.K. Chang, "Principle of Pictorial Information Systems Design", *Prentice-Hall, Inc.* 1989.